Available online at www.sciencedirect.com

SCIENCE DIRECT

Developmental Biology 278 (2005) 415–427

DEVELOPMENTAL BIOLOGY

www.elsevier.com/locate/ydbio

Retinoic acid-metabolizing enzyme Cyp26a1 is essential for determining territories of hindbrain and spinal cord in zebrafish

Yumi Emoto[a], Hironori Wada[b], Hitoshi Okamoto[b,c], Akira Kudo[a], Yoshiyuki Imai[a,*]

[a]*Department of Biological Information, Tokyo Institute of Technology, 4259 Nagatsuta-cho, Midori-ku, Yokohama 226-8501, Japan*
[b]*Laboratory for Developmental Gene Regulation, Brain Science Institute, RIKEN, 2-1 Hirosawa, Wako, Saitama 351-0198, Japan*
[c]*Core Research for Evolutional Science and Technology (CREST), Japan Science and Technology Corporation (JST), 4-1-8 Honcho, Kawaguchi, Saitama 332-0012, Japan*

Received for publication 17 August 2004, revised 9 November 2004, accepted 9 November 2004
Available online 15 December 2004

Abstract

Retinoic acid (RA) plays a critical role in neural patterning and organogenesis in the vertebrate embryo. Here we characterize a mutant of the zebrafish named *giraffe* (*gir*) in which the gene for the RA-degrading enzyme Cyp26a1 is mutated. The *gir* mutant displayed patterning defects in multiple organs including the common cardinal vein, pectoral fin, tail, hindbrain, and spinal cord. Analyses of molecular markers suggested that the lateral plate mesoderm is posteriorized in the *gir* mutant, which is likely to cause the defects of the common cardinal vein and pectoral fin. The *cyp26a1* expression in the rostral spinal cord was strongly upregulated in the *gir* mutant, suggesting a strong feedback control of its expression by RA signaling. We also found that the rostral spinal cord territory was expanded at the expense of the hindbrain territory in the *gir* mutant. Such a phenotype is the opposite of that of the mutant for Raldh2, an enzyme that synthesizes RA. We propose a model in which Cyp26a1 attenuates RA signaling in the prospective rostral spinal cord to limit the expression of *hox* genes and to determine the hindbrain–spinal cord boundary.

Keywords: *giraffe*; *neckless*; *cyp26a1*; *raldh2*; *hox*; Retinoic acid; Common cardinal vein; Hindbrain; Spinal cord; Zebrafish

Introduction

Retinoic acid (RA), a derivative of vitamin A, is an important signaling molecule for the morphogenesis of vertebrate embryos. All-*trans* RA is the major biologically active retinoid in vivo (Costaridis et al., 1996; Horton and Maden, 1995). This compound is present in embryonic and adult tissues at high levels and binds efficiently to retinoic acid receptors (RARs). All-*trans* RA is synthesized by way of two oxidation steps (for a review, see Perlmann, 2002). In the first step, vitamin A (retinol) is converted to all-*trans* retinaldehyde by alcohol dehydrogenases. In the second step, which is thought to be the rate-limiting one, all-*trans* retinaldehyde is converted to all-*trans* RA by any of three related aldehyde dehydrogenases, Raldh1, Raldh2, and Raldh3 (also known as Aldh1a1, Aldh1a2, and Aldh1a3, respectively). All-*trans* RA is in turn metabolized by members of the Cyp26 family of cytochrome *P*450 enzymes, which include Cyp26a1, Cyp26b1, and Cyp26c1. These enzymes convert all-*trans* RA to more polar metabolites, including 4-hydroxy-RA, 4-oxo-RA, 18-hydroxy-RA, and 5,8-epoxy-RA (Fujii et al., 1997; Taimi et al., 2004; White et al., 1996, 2000a). Although several assays have shown that these metabolites are biologically active (Idres et al., 2002 and references therein), genetic evidence has suggested that Cyp26a1 metabolites are not bioactive but merely degradation products (Niederreither et al., 2002).

Mutational analyses of the genes involved in the production and degradation of RA have been carried out in mouse and zebrafish. In mice, a loss of the *raldh2* function causes impaired body turning and heart looping,

* Corresponding author. Fax: +81 45 924 5718.
E-mail address: yimai@bio.titech.ac.jp (Y. Imai).

0012-1606/$ - see front matter © 2004 Elsevier Inc. All rights reserved.
doi:10.1016/j.ydbio.2004.11.023

shortening of the trunk region, absence of limb buds, hypoplastic otic vesicles, and lack of externally visible second and third branchial arches (Niederreither et al., 1999). Likewise, mutations in the *raldh2* gene in zebrafish named *neckless* (*nls*)/*no-fin* (*nof*) result in truncation of the anterior–posterior (AP) axis, defects in midline mesendodermal tissues, and absence of pectoral fins and cartilaginous gill arches (Begemann et al., 2001; Grandel et al., 2002). These phenotypes are similar to those of the vitamin A-deficient syndrome, suggesting that Raldh2 is the main source of RA produced during embryogenesis.

Targeted disruption of the mouse *cyp26a1* gene causes spina bifida, truncation of the tail, aplasia or hypoplasia of the urogenital system, posterior transformations of cervical vertebrae, and abnormal patterning of the rostral hindbrain (Abu-Abed et al., 2001; Sakai et al., 2001). Most of these phenotypes are similar to those induced by excess RA administration, suggesting that Cyp26a1 is essential for controlling the RA levels during embryogenesis. The early lethal phenotype of the *cyp26a1*-deficient mouse was rescued by heterozygous disruption of *raldh2*, suggesting that Cyp26a1 simply functions to protect the embryos from excess all-*trans* RA (Niederreither et al., 2002). In addition, a recent study on a *cyp26b1*-knockout mouse has revealed that the *cyp26b1* function is required for proximodistal patterning and outgrowth of the developing limb (Yashiro et al., 2004). In zebrafish, morpholino knockdown of *cyp26a1* caused anterior expansion of posterior genes such as *hoxb1b* and a reduction of the expression domain of the anterior gene *otx2* at the late gastrulation stage (Kudoh et al., 2002), suggesting that the Cyp26a1 function is required for the proper AP patterning of the neural ectoderm during gastrulation.

In this study, we isolated and characterized a novel mutant in zebrafish named *giraffe* (*gir*) that displays patterning defects in various organs including the common cardinal vein, pectoral fin, tail, hindbrain, and spinal cord. Expression patterns of *tbx5.1* and *raldh2* suggested that the lateral plate mesoderm is posteriorized in the *gir* mutant, and such a patterning defect is likely to cause the defective formation of common cardinal vein and pectoral fin. We show evidence that a loss of the *cyp26a1* function causes the *gir* phenotypes. As shown in *cyp26a1* knockdown embryos, the anterior neural ectoderm was reduced and the posterior neural ectoderm was expanded at the early stages in the *gir* mutant. We further show that the expression of the rostral spinal cord markers *hoxb5a* and *hoxb6a* were upregulated and expanded rostrally at the mid-segmentation stage in the *gir* mutant. A strong feedback regulation of the *cyp26a1* expression in the prospective rostral spinal cord is likely to be important for defining the rostral expression limit of these *hox* genes. We propose a model in which Cyp26a1 controls the RA level at the prospective rostral spinal cord and thereby plays a crucial role in territorial determination of the hindbrain and spinal cord.

Materials and methods

Fish and genetic procedures

The *gir* mutant was found in the background of another mutant *rw209* that is defective in jaw development (unpublished). The *rw209* mutant was identified in a genetic screen for mutations, in which a RIKEN strain carrying the *Islet-1* (*Isl1*)-GFP transgene (Higashijima et al., 2000) was mutagenized with *N*-ethyl-*N*-nitrosourea (ENU) (Masai et al., 2003). For mapping of *gir*, a *gir*/+ fish was crossed to a wild-type wik strain (Johnson and Zon, 1999; Nechiporuk et al., 1999); and the F1 progenies were then intercrossed to generate a panel of *gir*/*gir* embryos. Isolation of genomic DNA from embryos and mapping relative to SSLP markers were done as described previously (Gates et al., 1999; Knapik et al., 1998). To test directly the linkage between *gir* and *cyp26a1*, a *cyp26a1* fragment was amplified using primers 5′-CAGGGTTTGAGGGCACGCAATTT-3′ and 5′-GCTGCTTCTTTCATCGCCTAAGC-3′, and digested with *Xba*I, which cleaves the mutant *cyp26a1* allele, but not the wild-type allele.

In situ hybridization, histology, immunohistochemistry, and fluorescence microscopy

Whole mount in situ hybridization with digoxigenin-labeled RNA probes was done as described (Thisse et al., 1993). For sectioning, the stained embryos were fixed with 4% paraformaldehyde, embedded using Technovit 8100 (Kulzer) according to the manufacturer's instructionsm, and sectioned at 5 μm. Blood cells were stained with o-dianisidine according to Detrich et al. (1995). Alcian blue staining of cartilage tissue was performed as previously reported (Schilling et al., 1996). Acetylated α-tubulin antibody (Sigma, 1:1000 dilution) and a secondary antibody conjugated to Alexa-533 (Santa Cruz Biotechnology, 1:500 dilution) were used for immunofluorescence staining according to the standard protocol (Westerfield, 1995). Observations by fluorescence microscopy were made with a confocal microscope (Zeiss LSM 510).

Morpholino microinjection

A *cyp26a1* antisense morpholino (5′-CGCGCAACTGATCGCCAAAACGAAA-3′), which is complementary to −32 to −8 of the 5′ UTR of *cyp26a1* cDNA, a *raldh2* antisense morpholino (5′-GTTCAACTTCACTGGAGGTCATC-3′; Begemann et al., 2001; Grandel et al., 2002), and a standard control morpholino (5′-CCTCTTACCTCAGTTACAATTTATA-3′) were obtained from Gene Tools LLC. The morpholino solution (100 pl) in 5 mg/ml phenol red and 0.2 M KCl was microinjected into one- to eight-cell stage embryos using a pressurized microinjection device (PV820 Pneumatic Picopump, World Precision Instruments).

Results

The gir mutant is defective in the development of common cardinal veins

The phenotype of the *giraffe* (*gir*) mutant became apparent at 28 h postfertilization (hpf). At this stage, blood cells begin to circulate in wild-type embryos, whereas no circulation was observed in the *gir* mutant, although heart beating was observed. In addition, the *gir* mutant exhibited a shortened and distorted tail (Figs. 1A and B). During embryonic stages, the blood cells are produced in the intermediate cell mass (ICM), a region of the trunk ventral to the notochord, and then these cells enter the heart through the posterior cardinal vein and the common cardinal vein. In *gir* mutant embryos, blood cells accumulated in the posterior cardinal vein and failed to enter the common cardinal vein (Figs. 1C–F). Consequently, no or few blood cells were found in the dorsal aorta (Fig. 1D) or in the heart (Fig. 1F). By 3 days postfertilization (dpf), the *gir* mutant embryos exhibited severe edema (Figs. 1G and H) and eventually died within 1 week.

Since the *gir* mutant was defective in the initiation of blood cell circulation, we examined the expression of *flk1*, which marks endothelial cells, to ask if patterning of blood vessels was affected. Although most of the *flk1* expression was apparently normal, its expression in the common cardinal vein was absent in the *gir* mutant (Figs. 1I and J), suggesting that the defective formation of the common cardinal vein caused the failure of circulation in the *gir* mutant.

Patterning defects of pectoral fin and tail in the gir mutant

In addition to the defect in blood cell circulation, the *gir* mutation caused a patterning defect in the pectoral fins. At 36 hpf, fin bud formation was evident in wild-type embryos, whereas no fin bud was found in *gir* mutant embryos (Figs. 2A and B). At 3 dpf, no or small fins were observed in the *gir* mutant (Figs. 2C and D). We examined the expression of *tbx5.1*, which is expressed in the fin field and is essential for pectoral fin induction (Ahn et al., 2002; Garrity et al., 2002). At 20 hpf (~22-somite stage), the overall expression of *tbx5.1* was reduced in the *gir* mutant, and this reduction was prominent in the posterior region of

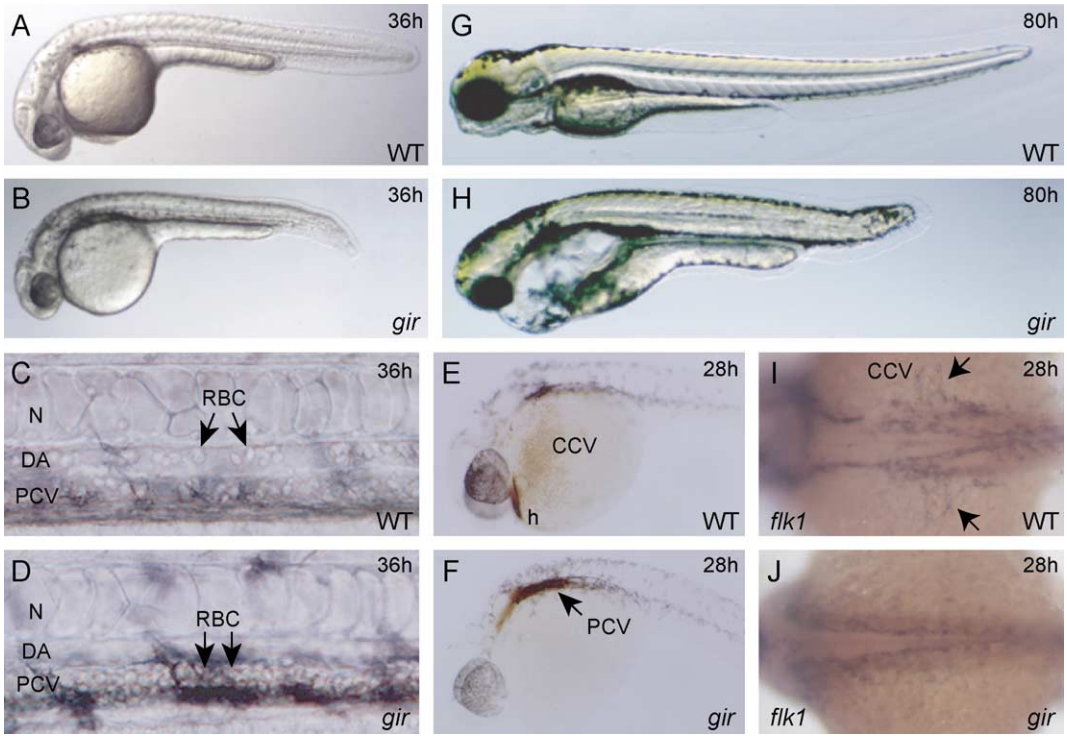

Fig. 1. Phenotypes of the *gir* mutant. (A and B) Morphology of the wild type (A) and *gir* mutant (B) embryos at 36 hpf. The *gir* mutant embryo exhibits a shortened tail. (C and D) Blood cells in dorsal aorta and posterior cardinal vein at 36 hpf. Circulating blood cells are evident in both dorsal aorta and posterior cardinal vein in wild-type embryos (C), whereas they are absent in the dorsal aorta and have accumulated in the posterior cardinal vein in *gir* mutant embryos (D). Photographs were taken after the embryos had been cooled on ice to make the circulation slower. (E and F) o-dianisidine staining of blood cells in wild type (E) and *gir* mutant (F) embryos at 28 hpf. Blood cells are seen in the common cardinal vein and heart in the wild-type embryo (E), whereas these cells have accumulated in the posterior cardinal vein and have failed to circulate in the *gir* mutant embryo (F). (G and H) Morphology of the wild-type (G) and *gir* mutant (H) embryos at 80 hpf. The *gir* mutant shows severe edema. (I and J) Expression of *flk1* at 28 hpf. *flk1* is expressed in the blood vessels including the common cardinal vein in wild-type embryo (I), whereas its expression is absent in the common cardinal vein of the *gir* mutant embryo (J). The arrows indicate the common cardinal vein. CCV, common cardinal vein; DA, dorsal aorta; h, heart; N, notochord; PCV, posterior cardinal vein; RBC, red blood cells.

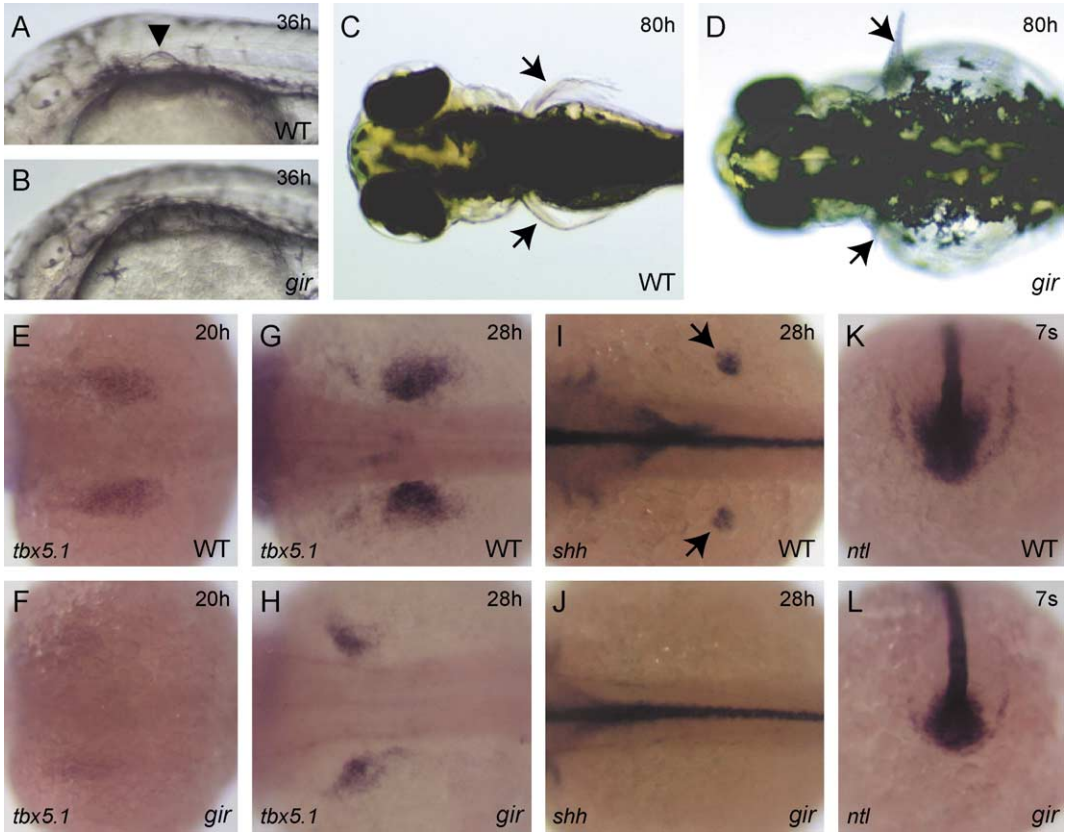

Fig. 2. Patterning defects in the pectoral fin bud and tailbud in the *gir* mutant. (A and B) Morphology of the pectoral fin bud in wild type (A) and *gir* mutant (B) embryos at 36 hpf. The arrowhead indicates the fin bud (A). The *gir* mutant embryo has no fin bud (B). (C and D) Dorsal views of the wild type (C) and *gir* mutant (D) embryos at 80 hpf. The arrows indicate pectoral fins. No or small fins were observed in the *gir* mutant embryo (D). (E–L) Expression of *tbx5.1* (E–H), *shh* (I and J), and *ntl* (K and L) was examined by in situ hybridization in wild type (E, G, I, and K) and *gir* mutant (F, H, J, and L) embryos. The expression domain of *tbx5.1* has shifted anteriorly in the *gir* mutant at 20 hpf (F) and 28 hpf (H). The fin bud expression of *shh* (shown by arrows in I) is absent in the *gir* mutant at 28 hpf (J). *ntl* expression is reduced in the tailbud of the *gir* mutant at the 7-somite stage (L). Genotypes were determined by PCR assay after the photographs had been taken in E, F, K, and L.

the fin field (Figs. 2E and F). At 28 hpf, *tbx5.1* expression in the mutant was found in a region of the lateral plate mesoderm anterior to the normal fin field (Figs. 2G and H). Expression of *shh*, a marker for zone of polarizing activity, was not detectable in the fin field of the *gir* mutant, although its expression in the midline was normal (Figs. 2I and J).

Since the *gir* mutant exhibited a defect in tail development (Figs. 1B and H), we examined the expression of *no tail* (*ntl*), the zebrafish ortholog of *Brachyury*, which is essential for tail development (Schulte-Merker et al., 1994). As a result, we found that although *ntl* expression in the notochord was not significantly affected, its expression in the tailbud was reduced at segmentation stages in the *gir* mutant (Figs. 2K and L).

We also noted that the pharyngeal cartilages, in particular Meckel's cartilage, were malformed in the *gir* mutant (data not shown). However, at the early larval stages when the cartilages develop, the overall morphology of the *gir* mutant was distorted because of the severe edema (Fig. 1H). In addition, the *gir* mutant dies at these stages. Therefore, we did not study the cartilage phenotypes further.

Genetic and molecular analyses of gir

Genetic mapping localized *gir* to the vicinity of LG12 marker Z27025 (no recombinants among 280 meioses, see Materials and methods). By searching for genes and ESTs that have been mapped to the genomic region around Z27025, we found *cyp26a1* and its EST clone fb81e05 on the HS meiotic map (Woods et al., 2000) and T51 radiation hybrid map (Geisler et al., 1999), respectively (Fig. 3A; http://zfin.org). *cyp26a1* was considered to be a good candidate for *gir*, since this gene has been shown to be important for patterning in mouse embryos (Abu-Abed et al., 2001; Sakai et al., 2001). We sequenced the RT-PCR fragment of this gene and found a nonsense mutation at position 814 (Glu272Stop; Fig. 3B). Accordingly, the truncated Cyp26a1 protein produced in the *gir* mutant lacks the heme-binding motif in the C-terminus, which is conserved among members of the cytochrome *P*450 superfamily (Fig. 3C; Graham-Lorence and Peterson, 1996), suggesting that the mutant Cyp26a1 protein is nonfunctional. By taking advantage of a restriction site polymorphism generated by the mutation, we found that

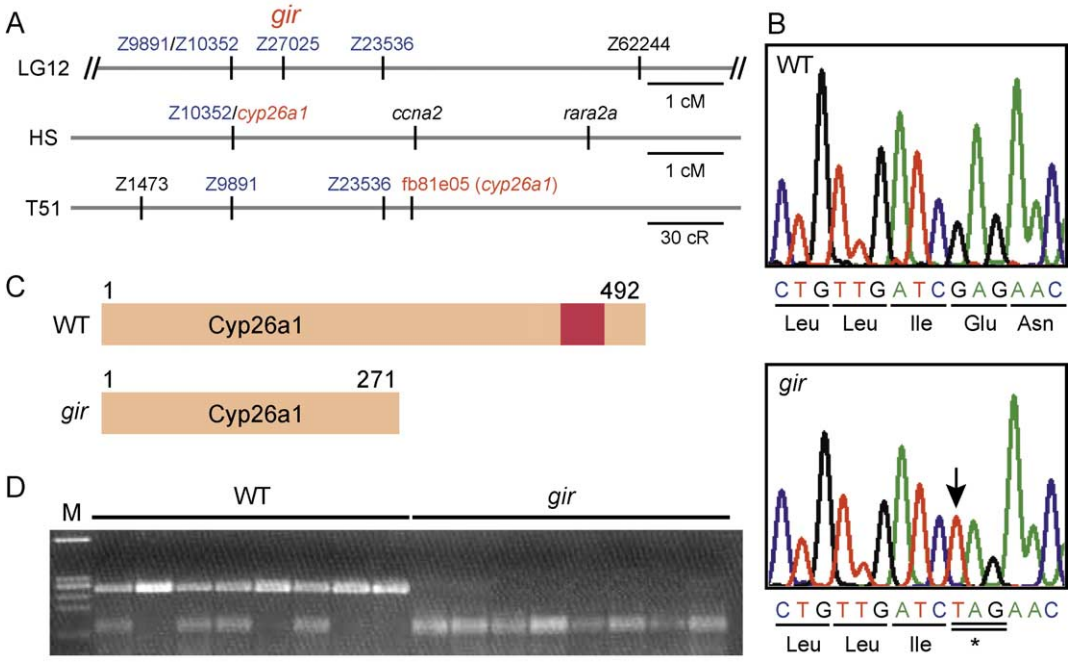

Fig. 3. Molecular isolation of *gir*. (A) Genetic mapping of *gir*. In our mapping panel, *gir* was mapped between Z9891/Z10352 and Z23536 (0.7 cm from Z9891/Z10352 and 1.3 cm from Z23536, $n = 150$) and at the same position as Z27025. In HS panel, the *cyp26a1* gene has been mapped at the same position as Z10352. In the T51 panel, fb81e05, an EST clone of *cyp26a1*, has been mapped near Z23536. (B) The *gir* mutant carries a nonsense mutation in the *cyp26a1* gene at position 814. The mutated nucleotide is indicated by the arrow. (C) Schematic representation of the Cyp26a1 protein and its truncated form in the *gir* mutant. The red box represents a heme-binding motif, which is conserved among cytochrome *P*450s. (D) The *cyp26a1* gene is linked to *gir*. A *cyp26a1* fragment was amplified from the wild-type (+/+ or *gir*/+) and *gir* mutant embryos and digested with *Xba*I, which cleaves the mutant *cyp26a1* allele, but not the wild-type allele. All *gir* mutants had only the mutant *cyp26a1* allele (no recombinants among 356 meioses), indicating that *cyp26a1* is tightly linked to *gir*.

cyp26a1 was tightly linked to *gir* (no recombinants among 356 meioses; Fig. 3D).

A cyp26a1 morpholino phenocopies the gir mutant

To confirm that *gir* encodes Cyp26a1, we injected a *cyp26a1* antisense morpholino (*cyp26a1*-MO) into wild-type embryos. Embryos injected with 1 ng of *cyp26a1*-MO exhibited a shortened tail (Figs. 4A and B), no or small pectoral fins (Figs. 4C and D), and defect in blood cell circulation (Figs. 4E and F), thus phenocopying the *gir* mutant. We noted that some of the *cyp26a1* morphants displayed a milder circulation defect than the *gir* mutant, such that blood cells entered the common cardinal vein and moved across the yolk to around the inflow tract, but did not circulate further (data not shown). Eighty-three out of 104 embryos injected with *cyp26a1*-MO phenocopied the *gir* mutant, whereas none of the 48 embryos injected with the control morpholino exhibited any of these phenotypes. Together with the mutational analysis described above, these results indicate that a loss of *cyp26a1* function causes the *gir* phenotypes.

Genetic interaction between gir/cyp26a1 and raldh2

Since Cyp26a1 is an enzyme that degrades RA, we speculated that an increased RA concentration caused the *gir* phenotypes. To confirm this hypothesis, we injected a *raldh2* antisense morpholino (*raldh2*-MO) into the *gir* mutant. Previous studies have shown that injection of 8.5–17 ng (Begemann et al., 2001) or 4 ng (Grandel et al., 2002) of *raldh2*-MO phenocopies the *nls*/*nof* mutant. In our experiments, injection of 4 ng of *raldh2*-MO partly phenocopied the *nls*/*nof* mutant: 59% (17/29) of the injected embryos exhibited complete loss of the pectoral fin and 34% (10/29) exhibited partial loss of the pectoral fin. We found that injection of 4 ng of *raldh2*-MO rescued the phenotypes of the *gir* mutant (Figs. 4G–L). Thirty-five out of 36 *gir* mutants injected with *raldh2*-MO exhibited normal tail morphology (Figs. 4G and H) and normal blood circulation (Figs. 4K and L). In addition, the pectoral fin defect was also partly rescued: 5 out of 36 mutants had apparently normal pectoral fins (Figs. 4I and J). Injection of 0.5 ng of *raldh2*-MO had only a mild effect on the wild-type embryos, but this efficiently rescued the circulation defects, but not the pectoral fin or tail defect, of the *gir* mutant (data not shown). These results suggest that a reduction of the RA level is sufficient to suppress the phenotypes of the *gir* mutant.

Expression of the cyp26a1 and raldh2 genes is affected in the gir mutant

It has been shown that expression of *cyp26a1* is upregulated by RA, whereas that of *raldh2* is down-

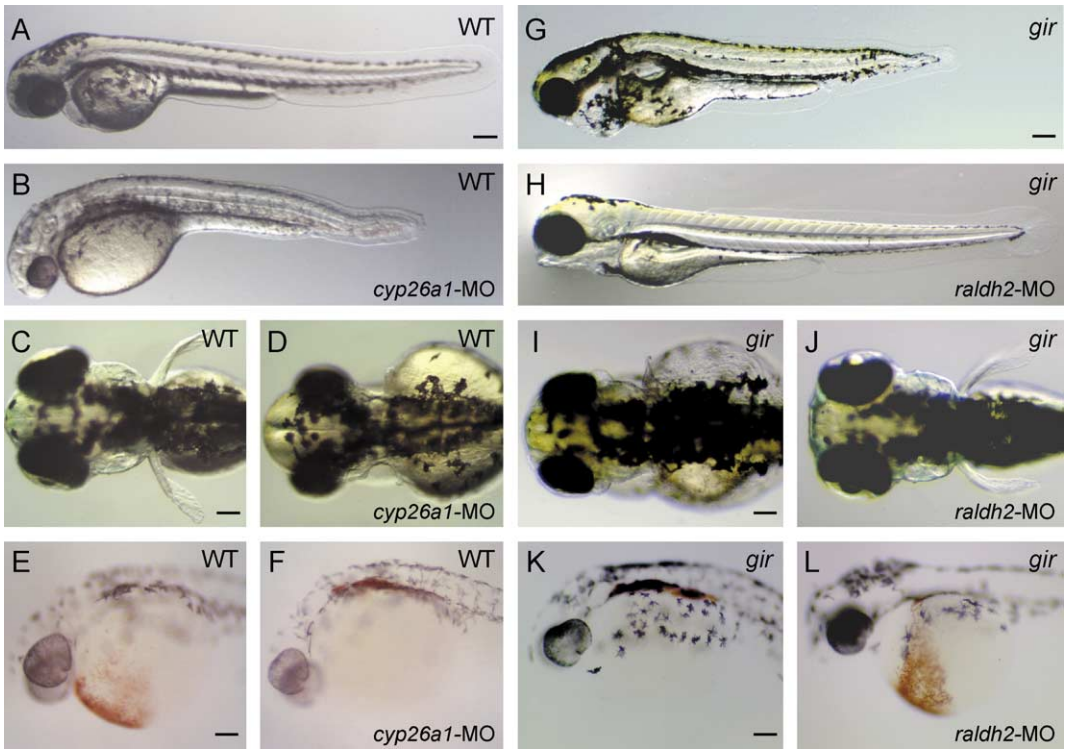

Fig. 4. Morpholino knockdown of *cyp26a1* and genetic interaction between *gir*/*cyp26a1* and *raldh2*. (A, C, and E) Uninjected wild-type control embryos and (B, D, and F) wild-type embryos injected with 1 ng *cyp26a1*-MO. (A and B) Lateral views of the embryos at 48 hpf. (C and D) Dorsal views of the embryos at 80 hpf. (E and F) o-dianisidine staining of blood cells of the embryos at 28 hpf. Phenotypes of the *cyp26a1* morphant are similar to those of the *gir* mutant. (G, I, and K) Uninjected *gir* mutants and (H, J, and L) *gir* mutants injected with 4 ng *raldh2*-MO. (G and H) Lateral views of the embryos at 80 hpf. (I and J) Dorsal view of the embryos at 80 hpf. (K and L) o-dianisidine staining of blood cells of the embryos at 48 hpf. Genotypes were determined by PCR assay after the photographs had been taken in H, J, and L.

regulated by RA (Begemann et al., 2001; Dobbs-McAuliffe et al., 2004; Kudoh et al., 2002). Therefore, we expected that expression of these genes might be altered in *gir* mutant embryos. The *cyp26a1* gene is expressed in the presumptive anterior neural ectoderm and around the blastoderm margin during gastrulation, in the tailbud throughout somitogenesis, and in multiple specific tissue types after the mid-segmentation stage (Dobbs-McAuliffe et al., 2004; Kudoh et al., 2002). We found that *cyp26a1* expression was not significantly affected during gastrulation stage and at bud stage (10 hpf) in the *gir* mutant (Figs. 5A and B). However, at the early segmentation stage when *cyp26a1* began to be expressed in the rostral presumptive spinal cord, its expression was upregulated in the *gir* mutant (Figs. 5C and D). Interestingly, *cyp26a1* expression in the rostral spinal cord was strongly upregulated at 20 hpf in the *gir* mutant (Figs. 5E and F). A transverse section confirmed that *cyp26a1* was expressed in the rostral spinal cord at this stage (Fig. 5G). Its expression was also upregulated and expanded in the tailbud of the *gir* mutant (Figs. 5E and F). At 28 hpf, *cyp26a1* expression in the caudal part of the branchial arch primordium was upregulated, whereas that in the rostral branchial arch primordium was slightly reduced in the *gir* mutant (Figs. 5H and I).

Expression of the *raldh2* gene was also altered in the *gir* mutant. During gastrulation stages, *raldh2* expression in the blastoderm margin was only slightly, if at all, reduced in the *gir* mutant (data not shown). At bud stage, its expression in the presomitic mesoderm was significantly reduced in the *gir* mutant (Figs. 5J and K). At 20 hpf, *raldh2* expression in the somites was downregulated in the *gir* mutant (Figs. 5L and M). At 28 hpf, the *raldh2* expression domain in the caudal part of the branchial arch primordium was slightly narrowed (Figs. 5N and O). Interestingly, its expression domain in the lateral plate mesoderm including the posterior pectoral fin field was strongly expanded rostrally in the *gir* mutant (Figs. 5N and O). These results suggest that the *gir* mutation alters the RA distribution in embryos, which subsequently affects expression patterns of *cyp26a1* and *raldh2*.

Patterning defects of hindbrain in the gir mutant

We asked if the *gir* mutation affects patterning of the hindbrain, since decreased or increased RA signaling affects hindbrain development in zebrafish (Begemann et al., 2001, 2004; Grandel et al., 2002; Hill et al., 1995; Holder and Hill, 1991; Linville et al., 2004; Perz-Edwards et al., 2001). Expressions of *krox20*, which marks rhombomeres 3 and 5, and that of *valentino*, which is expressed in rhombomeres 5 and 6, were

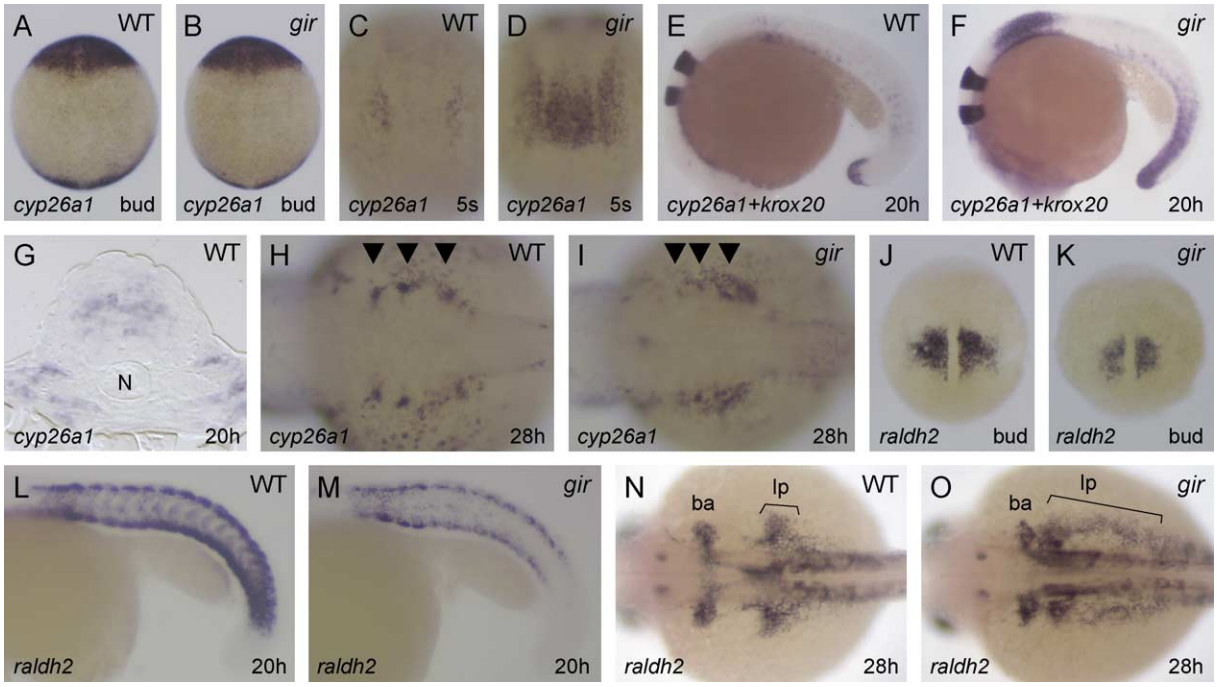

Fig. 5. Expression of *cyp26a1* and *raldh2* is affected in the *gir* mutant. Expression of *cyp26a1* (A–D and G–I), *cyp26a1* and *krox20* (E and F), and *raldh2* (J–O) in the wild type (A, C, E, G, H, J, L, and N) and *gir* mutant (B, D, F, I, K, M, and O) embryos. (A and B) *cyp26a1* expression in the presumptive anterior neural ectoderm and in the tailbud is little affected at bud stage in the *gir* mutant. Dorsal views are shown. (C and D) At the 5-somite stage, *cyp26a1* expression in the rostral presumptive spinal cord is upregulated in the *gir* mutant. (E and F) At 20 hpf, *cyp26a1* expression is strongly upregulated in the rostral spinal cord and in the tailbud of the *gir* mutant. (G) A transverse section at the level of the rostral spinal cord showing *cyp26a1* expression in the wild-type embryo at 20 hpf. N, notochord. (H and I) *cyp26a1* expression in the developing branchial arches (indicated by the arrowheads) is perturbed at 28 hpf in the *gir* mutant. (J–M) *raldh2* expression in the presomitic mesoderm and in the somites is reduced in the *gir* mutant at bud stage (K) and 20 hpf (M). (N and O) At 28 hpf, *raldh2* expression in the posterior branchial arch primordium (ba) and in the posterior fin bud- and lateral plate-mesoderm (lp) is disturbed in the *gir* mutant. Genotypes were determined by PCR assay after the photographs had been taken in A–F and J–M.

examined together with *myoD*, a marker for somites. Interestingly, the spacing between rhombomere 5 or 6 and the first somite was significantly expanded at the mid-segmentation stages in the *gir* mutant (Figs. 6A–D). In addition, we noticed that the expression domain of *valentino* was reduced in the *gir* mutant (Figs. 6C and D). By examining expression of *pax2.1*, a marker for the midbrain–hindbrain boundary, together with *krox20*, we found that the spacing between the midbrain–hindbrain boundary and rhombomere 3 was reduced in the *gir* mutant (Figs. 6E and F), indicating that the rostral hindbrain territory was reduced. Likewise, the spacing between rhombomere 1, which is marked by *gbx2*, and rhombomere 3 was slightly reduced in the *gir* mutant (Figs. 6G and H). We examined an additional gene *eph-b2* that has multiple expression domains including rhombomeres 4 and 7 and somites. We found that the spacing between rhombomere 7 and the first somite was expanded in the *gir* mutant (Figs. 6I and J). These phenotypes were opposite to those of the *nls*/*nof* mutant, in which the spacing between rhombomere 5 and the first somite is reduced, the expression domain of *valentino* is expanded, and the rostral hindbrain territory is expanded (Begemann et al., 2001; Grandel et al., 2002).

To study patterning of more rostral structures, we also examined *otx2*, which is expressed mainly in the midbrain and in the part of diencephalon beneath the epiphysis at the mid-segmentation stages. The *otx2* expression domain in the midbrain was found to be reduced (Figs. 6K and L), suggesting that the midbrain territory was reduced in the *gir* mutant. Furthermore, the *otx2* expression pattern suggested that the forebrain territory of the mutant was also reduced (Figs. 6K and L).

Patterning defects of spinal cord in the gir mutant

Next, we examined expression of neural tube markers *hoxb4a*, *hoxb5a*, and *hoxb6a*, which have their rostral expression limit at the rhombomere 6/7 boundary, at the level of somite 1 and at the level of somite 2, respectively (Prince et al., 1998a,b). It should be noted that *hoxb5*, the tetrapod ortholog of *hoxb5a*, has been often used as a marker for the rostral edge of the spinal cord after approximately 12-somite stage (White et al., 2000b and refereces therein). We found that expression of these *hox* genes was strongly upregulated at 20 hpf in the *gir* mutant (Figs. 7A–F). Furthermore, the spacing between the expression domains of *krox20* and *hoxb5a* or *hoxb6a* was strongly reduced (Figs. 7C–F). This is in contrast to

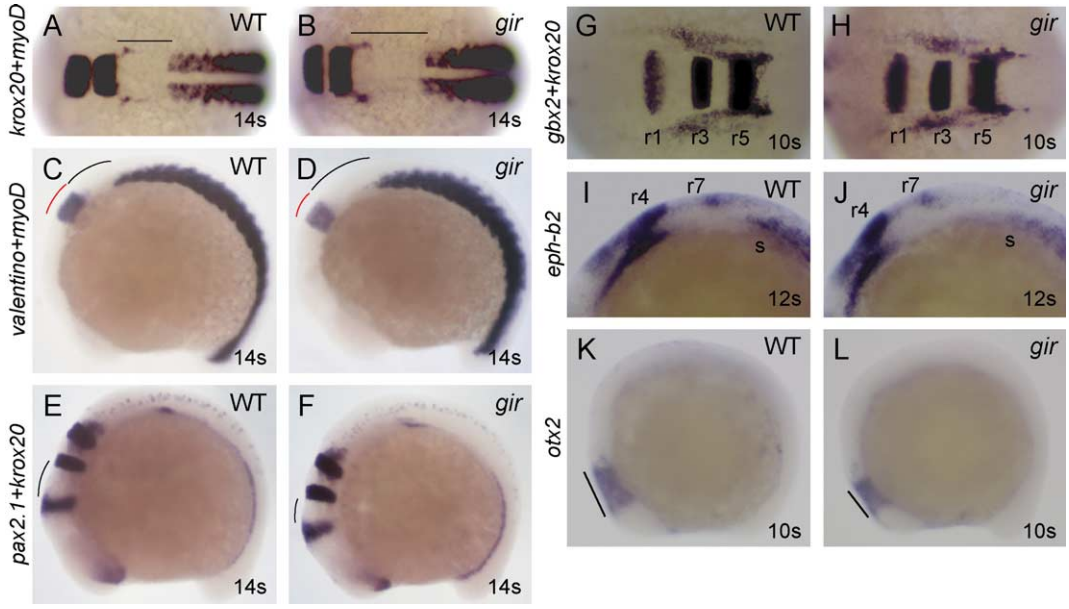

Fig. 6. Patterning of hindbrain is affected in the *gir* mutant. Expression of *krox20* and *myoD* (A and B), *valentino* and *myoD* (C and D), *pax2.1* and *krox20* (E and F), *gbx2* and *krox20* (G and H), *eph-b2* (I and J), and *otx2* (K and L) in wild type (A, C, E, G, I, and K) and *gir* mutant (B, D, F, H, J, and L) embryos. (A–D) The distance between the rhombomere 5 (*krox20*) or 6 (*valentino*) and the first somite is expanded, and the expression domain of *valentino* is reduced, in the *gir* mutant at the 14-somite stage. (E and F) The distance between midbrain–hindbrain boundary (*pax2.1*) and rhombomere 3 (*krox20*) is reduced in the *gir* mutant at the 14-somite stage. (G and H) The distance between rhombomere 1 (*gbx2*) and rhombomere 3 (*krox20*) is slightly reduced in the *gir* mutant at the 10-somite stage. (I and J) The distance between rhombomere 7 and the first somite is expanded in the *gir* mutant at the 12-somite stage. (K and L) The *otx2* expression domain in the midbrain was reduced in the *gir* mutant at the 10-somite stage. Dorsal views (A, B, G, and H) and lateral views (C–F and I–L) are shown. Genotypes were determined by PCR assay after the photographs had been taken. r, rhombomere; s, somites.

the expanded spacing between the expression domains of *krox20* and *myoD* (Figs. 6A and B). These analyses demonstrate that the spinal cord territory is expanded rostrally at the expense of the hindbrain territory in the *gir* mutant.

Patterning defects of motor neurons in the gir mutant

The *gir* mutant line carried the *Isl1*-GFP transgene (see Materials and methods), which is expressed in postmitotic motor neurons early in their development (Higashijima et al., 2000). Using this *Isl1*-GFP transgene, we studied development of motor neurons in the hindbrain and rostral spinal cord. We found that the distance between the trochlear nucleus (nIV) in the midbrain and the trigeminal nucleus (nV) in the rhombomeres 2/3 was reduced in the *gir* mutant at 48 hpf (Figs. 8A–C), consistent with the reduction in the rostral hindbrain territory. In some cases, the number of branchiomotor neurons in the trigeminal nucleus (nV) was reduced in the *gir* mutant (Fig. 8C). In addition, bilateral clusters of the vagal nucleus (nX) were found to have broadened (Figs. 8A–C). Despite the abnormal vagal nucleus patterning, projection of the vagal axons was apparently normal in the *gir* mutant (Figs. 8D and E).

At 3 dpf, *Isl1*-GFP-positive spinal motor neurons projected their axons dorsally in wild-type embryos (Fig. 8F). However, the axon projection of the rostralmost spinal motor neurons was not seen in the *gir* mutant (Fig. 8G). To study further the neuronal development in this region, we stained the embryos with acetylated α-tubulin antibody. By this assay, the spinal motor neurons projecting their axons ventrolaterally were detected (Figs. 8H and I). We found that the α-tubulin-positive motor neurons in the rostralmost spinal cord extended their axons even in the absence of the target pectoral fin bud (Figs. 8H and I), in contrast to the absence of axons from *Isl1*-GFP-positive motor neurons in this region. These results indicate that a subset of motor neurons was more selectively affected than others in the *gir* mutant.

Discussion

In this study, we characterized the *gir* mutant in zebrafish, which shows pleiotropic phenotypes, including defects in the development of common cardinal vein, pectoral fin, tail, hindbrain, and spinal cord. Genetic analysis and the results of the gene knockdown experiment using morpholino oligonucleotides demonstrate that loss of *cyp26a1* gene function causes the *gir* phenotypes. Cyp26a1 is an enzyme that degrades RA (Fujii et al., 1997; White et al., 1996), suggesting that RA concentration is increased in the *gir* mutant. Consistent with this hypothesis, injection of *raldh2*-MO, which is supposed to reduce the RA level (Begemann et al., 2001; Grandel et al., 2002), rescued the phenotypes of the *gir* mutant (Figs. 4G–L).

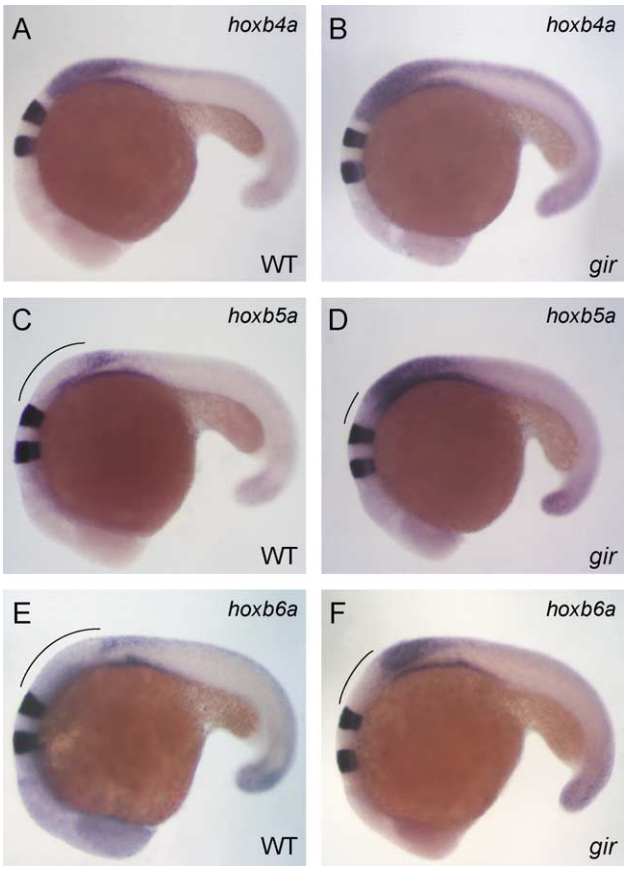

Fig. 7. Patterning of the spinal cord is affected in the *gir* mutant. Expression of *hoxb4a* and *krox20* (A and B), *hoxb5a* and *krox20* (C and D), and *hoxb6a* and *krox20* (E and F) in wild type (A, C, and E) and *gir* mutant (B, D, and F) embryos at 20 hpf. Expression of these *hox* genes is upregulated and the expression domains of *hoxb5a* and *hoxb6a* are markedly expanded rostrally in the *gir* mutant. Genotypes were determined by PCR assay after the photographs had been taken.

Phenotypic similarities and differences between the gir/cyp26a1 mutant and the cyp26a1-knockout mouse

Phenotypes of *gir* mutant embryos are similar to those of the *cyp26a1*-knockout mouse, but there are important differences. One of the common phenotypes is the tail truncation. Both the mouse and zebrafish *cyp26a1* genes are strongly expressed in the tailbud mesoderm at the segmentation stages, and mutations in both species cause the defect in tail development, concomitant with the reduction in *Brachyury*/*ntl* expression. Thus, RA degradation by Cyp26a1 in the tailbud is essential for the normal tail morphogenesis both in mouse and zebrafish.

Some of the phenotypic differences between the mouse and zebrafish *cyp26a1* mutants may be partly due to developmental differences between the two species. For example, the mouse mutant exhibits sirenomelia (fusion of the hindlimbs), but such a phenotype cannot be observed in the *gir* mutant, because the hindlimbs start to develop during metamorphosis, to which stage the *gir* mutant is unable to survive. Moreover, the *gir* mutant failed to initiate circulation due to the defective common cardinal vein formation on the surface of the yolk; whereas such a phenotype has not been reported in *cyp26a1*-knockout mouse. Development and morphology of the blood vessels, especially those of the yolk vessels, are highly divergent between mouse and zebrafish, and such differences are likely to result in phenotypic differences.

In addition, some of the phenotypic differences might be accounted for by gene redundancy and different gene expression patterns. Three members of the *cyp26* gene family, *cyp26a1*, *cyp26b1*, and *cyp26c1*, have been identified in mice; and the expression patterns of these genes were found to partly overlap (Abu-Abed et al., 2002; MacLean et al., 2001; Tahayato et al., 2003). Similarly, the zebrafish genome harbors at least three members of this family, including *cyp26a1* and *cyp26b1* (Nelson, 1999; White et al., 1996; our unpublished data). Although the expression pattern of the zebrafish *cyp26b1* gene has not been reported yet, functional redundancy among the members of this family might be different between the mouse and zebrafish. It should be noted that the expression pattern of the *cyp26a1* gene is significantly different between mouse and zebrafish. For example, mouse *cyp26a1* is expressed transiently in the prospective rhombomere 2, but is not expressed in the prospective rostral spinal cord (Fujii et al., 1997). In contrast, zebrafish *cyp26a1* is expressed in the prospective rostral spinal cord but not in the prospective rhombomere 2. Consistently, the mouse and zebrafish *cyp26a1* mutants display different phenotypes with respect to patterning in the hindbrain and spinal cord (see below).

Cyp26a1 function is required for the development of the common cardinal vein and pectoral fin

We showed that the *cyp26a1* function is required for the development of the common cardinal vein, which is an unusually broad vessel, covering a large portion of the yolk surface. RA signaling has been implicated in the formation of vitelline vessels and the cardiac inflow tract in murine and avian embryos. Vitamin A-deficient quail embryos exhibit the absence of omphalomesenteric veins, as well as the absence of sinus venosa and atria (Heine et al., 1985). In addition, *raldh2*-knockout mouse embryos lacked an organized network of extraembryonic vessels in their yolk sac membranes (Niederreither et al., 1999). Thus, RA signaling seems to play an important role in the development of blood vessels on the yolk in both zebrafish and higher vertebrates. Although little is known about the molecular mechanisms regulating the development of the common cardinal vein, we speculate that patterning defects in the lateral plate mesoderm (discussed below) might cause the failure of the common cardinal vein development in the *gir* mutant.

The *gir* mutant displays a severe defect in the development of its pectoral fin buds, equivalent to

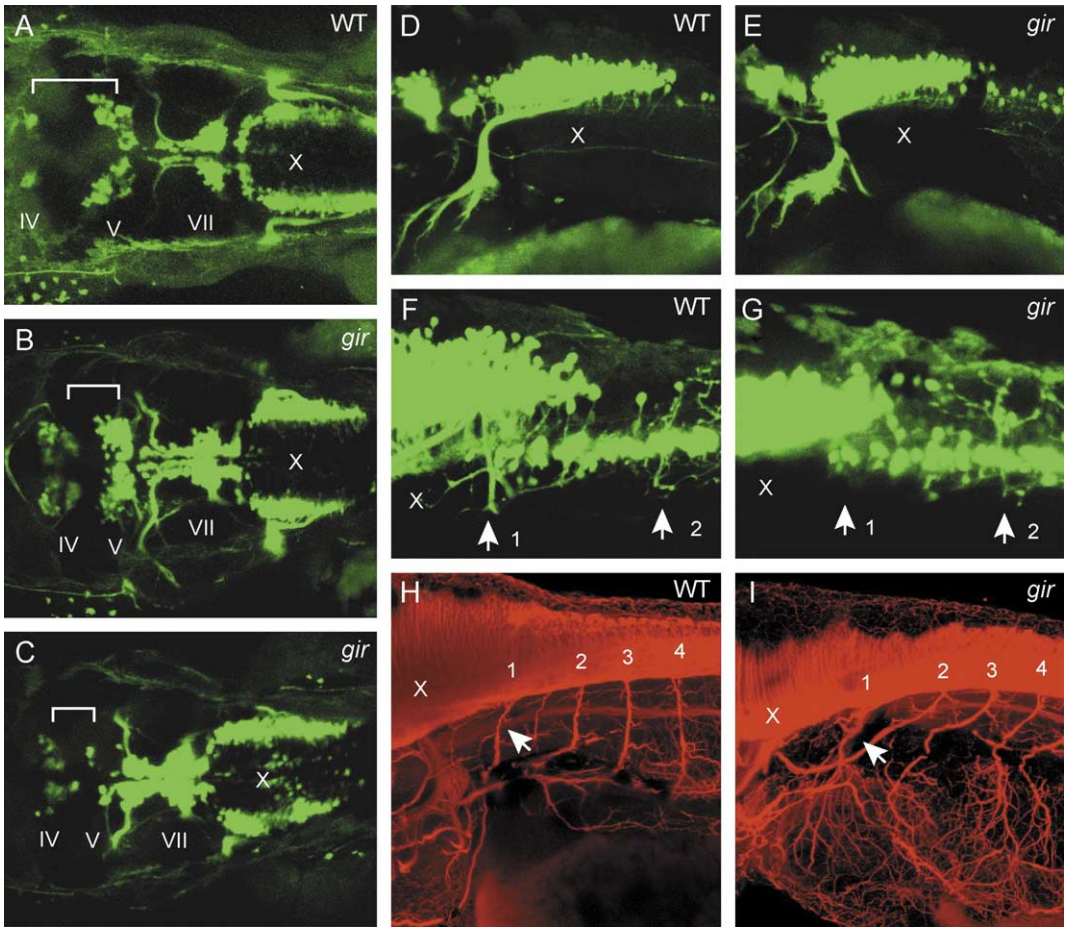

Fig. 8. Patterning of motor neurons is affected in the *gir* mutant. (A–G) Expression of the *Isl1*-GFP transgene was examined by fluorescence microscopy. (A–E) Dorsal views of hindbrain (A–C) and lateral views of caudal hindbrain and rostral spinal cord (D and E) in wild type (A and D) and *gir* mutant (B, C, and E) embryos at 48 hpf. The distance between the trochlear (nIV) and trigeminal (nV) nuclei is reduced, and bilateral clusters of the vagal nucleus (nX) are broadened, in the *gir* mutant (B and C). In some of the *gir* mutants, the number of neurons in the trigeminal nucleus (nV) is reduced (C). (F and G) Lateral views of caudal hindbrain and rostral spinal cord in wild type (F) and *gir* mutant (G) embryos at 3 dpf. Dorsal projection of motor neuron axons in the rostralmost spinal cord (labeled by arrow 1) is absent in the *gir* mutant (G). (H and I) Immunostaining of motor neurons with acetylated α-tubulin antibody in the caudal hindbrain and rostral spinal cord of wild type (H) and *gir* mutant (I) embryos at 3 dpf. Axons of spinal motor neurons are not significantly affected in the *gir* mutant (I). Arrows indicate axons from the rostralmost spinal motor neurons.

forelimb buds in higher vertebrates (Figs. 2A–D). This result was rather surprising, because RA signaling has been shown to be sufficient and necessary for the induction of a zone of polarizing activity in the developing limb bud (Helms et al., 1996; Stratford et al., 1996; Tickle et al., 1982). In the *gir* mutant, the expression domain of *tbx5.1* was shifted anteriorly and that of *raldh2* was expanded anteriorly (Figs. 2E–H and 5N and O), suggesting that the lateral plate mesoderm is posteriorized. Such a patterning defect of the lateral plate mesoderm is likely to cause the defective fin bud development. It has been suggested that the early expression of *hox* genes in the lateral plate mesoderm along the body axis specifies positions where limbs develop (Cohn et al., 1997). Considering this, the altered RA distribution in the *gir* mutant might affect the expression of *hox* genes in the lateral plate mesoderm, which might subsequently cause the defect in specification of the fin field.

RA signaling determines the territories of hindbrain and spinal cord

Because expression of the *cyp26a1* gene is induced by RA (Dobbs-McAuliffe et al., 2004; Kudoh et al., 2002), we expected to be able to monitor the RA distribution partly by examining the expression of *cyp26a1*. Surprisingly, the *cyp26a1* expression was highly upregulated in the prospective rostral spinal cord in the *gir* mutant (Figs. 5C–F), suggesting that a strong feedback control mechanism regulates its expression in this region. Supposing this *cyp26a1* expression to be induced by RA, a considerable amount of RA may be accumulated in the prospective rostral spinal cord. This RA accumulation would likely cause the patterning defects in the hindbrain and spinal cord.

cyp26a1 is expressed in the prospective forebrain and midbrain with a posterior limit around the future rhombomere 1 during gastrulation and at the early segmentation stage (Dobbs-McAuliffe et al., 2004; Kudoh et al., 2002).

As shown in *cyp26a1* knockdown embryos (Kudoh et al., 2002), the expression domain of the anterior gene *otx2* was reduced and that of the posterior gene *hoxb1b* was expanded at the late gastrulation stage in the *gir* mutant (data not shown). We also found that the territories of the forebrain and midbrain were reduced at the mid-segmentation stage in the *gir* mutant (Figs. 6K and L). Accordingly, the early expression of *cyp26a1* seems to be important for the proper AP patterning of the neural ectoderm, as suggested previously (Kudoh et al., 2002). Although the AP patterning defect of the mutant is likely to be caused by an increased RA concentration, the *cyp26a1* expression was not significantly affected by bud stage in the *gir* mutant (Figs. 5A and B), suggesting that the early *cyp26a1* expression is less sensitive to the altered RA concentration. However, its expression was strongly upregulated in the prospective rostral spinal cord at the 5-somite stage (Figs. 5C and D). *cyp26a1* expression in this region seems to be important to define the rostral limit of the spinal cord territory.

Several lines of evidence have suggested that diffusion of RA from the paraxial mesoderm to the neural tube is important to activate the *hox* genes and to pattern the hindbrain (reviewed in Gavalas, 2002). It has been also shown that the murine *hoxb5*, *hoxb6*, and *hoxb8* genes rapidly respond to exogenous RA to extend their expression domains rostrally (Oosterveen et al., 2003), suggesting that these *hox* genes are directly regulated by RA signaling. Based on these findings, we propose the following model (Fig. 9): RA is produced in the somitic mesoderm and diffuses into the prospective spinal cord, where it activates the expression of *hox* genes, including *hoxb5a* and *hoxb6a*. Cyp26a1 is expressed in the prospective rostral spinal cord, where it degrades RA, thus attenuating RA signaling (Fig. 9A). In the *gir* mutant, the RA level cannot be lowered at the prospective rostral spinal cord, causing expanded expression domains of these *hox* genes. As a result, the territory of the rostral spinal cord is expanded at the expense of that of the hindbrain (Fig. 9B). In contrast, when the RA level is reduced by mutations in the *raldh2* gene, the opposite phenotype is observed, that is, the hindbrain territory is expanded at the expense of the rostral spinal cord territory (Begemann et al., 2001; Grandel et al., 2002). Thus, the RA level at the rostral spinal cord is crucial to determine the territories of the hindbrain and spinal cord.

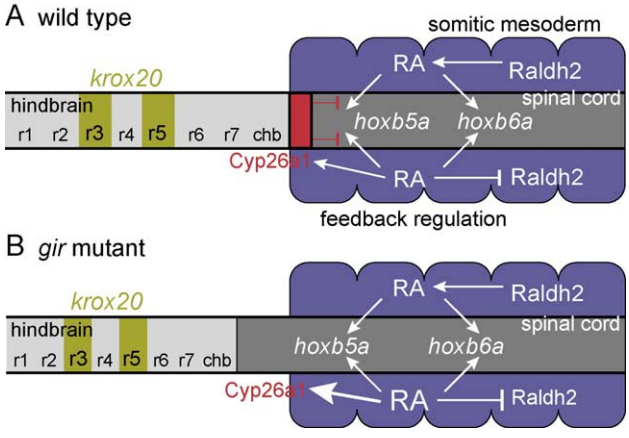

Fig. 9. A model for the role of Cyp26a1 in patterning the hindbrain and rostral spinal cord. (A) RA is produced in somites and diffuses into the prospective spinal cord, where it activates the expression of *hoxb5a* and *hoxb6a*. Cyp26a1 degrades RA in the prospective rostral spinal cord to limit the expression of these *hox* genes. (B) In the absence of *cyp26a1* function, the expression domains of *hoxb5a* and *hoxb6a* are expanded rostrally. Consequently, the territory of rostral spinal cord is expanded at the expense of the hindbrain territory. Expression of *cyp26a1* and *raldh2* is positively and negatively regulated, respectively, by RA. Accordingly, these genes are upregulated and downregulated, respectively, in the *gir* mutant. chb, caudalmost hindbrain; r1–r7, rhombomeres 1–7.

In our model, RA signaling activates *hox* genes, while Cyp26a1 protects the anterior central nervous system (CNS) from excessive exposure to RA. Interestingly, the inactivation of RA by Cyp26a1 apparently takes place at different positions within the CNS between zebrafish and higher vertebrates, because the mouse and chick *cyp26a1* is expressed in the prospective rhombomere 2, where it supposedly controls the RA level (Abu-Abed et al., 2001; Fujii et al., 1997; Sakai et al., 2001; Swindell et al., 1999). Consistently, the targeted disruption of the mouse *cyp26a1* gene causes misspecification of the rostral hindbrain, rather than rostral expansion of the spinal cord (Abu-Abed et al., 2001; Sakai et al., 2001). Furthermore, it should be noted that the *cyp26b1* and *cyp26c1* genes, other members of the *cyp26* family, are expressed at unique positions in the CNS: mouse *cyp26b1* is expressed throughout rhombomeres 5–6, in the ventral portion of rhombomeres 2–4, and in the upper and lower thoracic regions of the spinal cord (Abu-Abed et al., 2002; MacLean et al., 2001); and mouse *cyp26c1* is expressed in rhombomeres 2 and 4 (Tahayato et al., 2003). Considering these expression patterns, members of the Cyp26 family are likely to control the RA level at the multiple discrete areas of the CNS. Further analyses of the expression and function of these *cyp26* genes will reveal the overall regulation of the RA level by the members of Cyp26 family in the CNS and in other organs.

The axons from Isl1-GFP-positive rostralmost spinal motor neurons are missing in the gir mutant

Early RA signaling is required for the development of motor neuron progenitors, whereas later RA signaling in postmitotic motor neurons appears to regulate their columnar subtype identity (reviewed in Appel and Eisen, 2003). Blockage of RA signaling in postmitotic brachial (forelimb) motor neurons inhibits lateral motor column differentiation and converts many of these neurons to thoracic columnar subtypes, whereas activation of RA signaling impairs the differentiation of thoracic motor neuron columnar subtypes (Sockanathan et al., 2003). Thus, the level of RA signaling apparently determines motor neuron columnar subtype identity. We found that the *Isl1*-GFP-positive motor

neurons, but not the acetylated α-tubulin-positive motor neurons, failed to extend their axons in the rostralmost spinal cord of the *gir* mutant (Figs. 8F–I). Since RA level is considered to be very high in the rostral spinal cord of the *gir* mutant, these *Isl1*-GFP-positive motor neurons may be unable to mature under high levels of RA signaling. Alternatively, maturation of these motor neurons might be dependent on some signal(s) other than RA, which is produced in the somitic mesoderm and diffuses into the neural tube. The expanded spacing between the rostralmost spinal cord and somitic mesoderm in the *gir* mutant can cause a reduction in such signal(s) in the rostralmost spinal cord and impair the signal-dependent maturation of motor neurons. Further study is required to identify the signals that direct maturation of the *Isl1*-GFP-positive motor neurons in the rostralmost spinal cord.

Acknowledgments

We thank Dr. W.S. Talbot for critical reading of the manuscript, and Drs. H. Takeda and K. Yamasu for providing us with plasmids. This work was supported by grants from RIKEN BSI and CREST, JST to HO, and grants-in-aid from the Ministry of Education, Culture, Sports, Science and Technology of Japan to AK and YI.

References

Abu-Abed, S., Dolle, P., Metzger, D., Beckett, B., Chambon, P., Petkovich, M., 2001. The retinoic acid-metabolizing enzyme, CYP26A1, is essential for normal hindbrain patterning, vertebral identity, and development of posterior structures. Genes Dev. 15, 226–240.

Abu-Abed, S., MacLean, G., Fraulob, V., Chambon, P., Petkovich, M., Dolle, P., 2002. Differential expression of the retinoic acid-metabolizing enzymes CYP26A1 and CYP26B1 during murine organogenesis. Mech. Dev. 110, 173–177.

Ahn, D.G., Kourakis, M.J., Rohde, L.A., Silver, L.M., Ho, R.K., 2002. T-box gene *tbx5* is essential for formation of the pectoral limb bud. Nature 417, 754–758.

Appel, B., Eisen, J.S., 2003. Retinoids run rampant: multiple roles during spinal cord and motor neuron development. Neuron 40, 461–464.

Begemann, G., Schilling, T.F., Rauch, G.J., Geisler, R., Ingham, P.W., 2001. The zebrafish neckless mutation reveals a requirement for *raldh2* in mesodermal signals that pattern the hindbrain. Development 128, 3081–3094.

Begemann, G., Marx, M., Mebus, K., Meyer, A., Bastmeyer, M., 2004. Beyond the neckless phenotype: influence of reduced retinoic acid signaling on motor neuron development in the zebrafish hindbrain. Dev. Biol. 271, 119–129.

Cohn, M.J., Patel, K., Krumlauf, R., Wilkinson, D.G., Clarke, J.D., Tickle, C., 1997. *Hox9* genes and vertebrate limb specification. Nature 387, 97–101.

Costaridis, P., Horton, C., Zeitlinger, J., Holder, N., Maden, M., 1996. Endogenous retinoids in the zebrafish embryo and adult. Dev. Dyn. 205, 41–51.

Detrich III, H.W., Kieran, M.W., Chan, F.Y., Barone, L.M., Yee, K., Rundstadler, J.A., Pratt, S., Ransom, D., Zon, L.I., 1995. Intra-embryonic hematopoietic cell migration during vertebrate development. Proc. Natl. Acad. Sci. U. S. A. 92, 10713–10717.

Dobbs-McAuliffe, B., Zhao, Q., Linney, E., 2004. Feedback mechanisms regulate retinoic acid production and degradation in the zebrafish embryo. Mech. Dev. 121, 339–350.

Fujii, H., Sato, T., Kaneko, S., Gotoh, O., Fujii-Kuriyama, Y., Osawa, K., Kato, S., Hamada, H., 1997. Metabolic inactivation of retinoic acid by a novel P450 differentially expressed in developing mouse embryos. EMBO J. 16, 4163–4173.

Garrity, D.M., Childs, S., Fishman, M.C., 2002. The heartstrings mutation in zebrafish causes heart/fin Tbx5 deficiency syndrome. Development 129, 4635–4645.

Gates, M.A., Kim, L., Egan, E.S., Cardozo, T., Sirotkin, H.I., Dougan, S.T., Lashkari, D., Abagyan, R., Schier, A.F., Talbot, W.S., 1999. A genetic linkage map for zebrafish: comparative analysis and localization of genes and expressed sequences. Genome Res. 9, 334–347.

Gavalas, A., 2002. Arranging the hindbrain. Trends Neurosci. 25, 61–64.

Geisler, R., Rauch, G.J., Baier, H., van Bebber, F., Bross, L., Dekens, M.P., Finger, K., Fricke, C., Gates, M.A., Geiger, H., Geiger-Rudolph, S., Gilmour, D., Glaser, S., Gnugge, L., Habeck, H., Hingst, K., Holley, S., Keenan, J., Kirn, A., Knaut, H., Lashkari, D., Maderspacher, F., Martyn, U., Neuhauss, S., Neumann, C., Nicolson, T., Pelegri, F., Ray, R., Rick, J.M., Roehl, H., Roeser, T., Schauerte, H.E., Schier, A.F., Schonberger, U., Schonthaler, H.-B., Schulte-Merker, S., Seydler, C., Talbot, W.S., Weiler, C., Nusslein-Volhard, C., Haffter, P., 1999. A radiation hybrid map of the zebrafish genome. Nat. Genet. 23, 86–89.

Graham-Lorence, S.E., Peterson, J.A., 1996. Structural alignments of P450s and extrapolations to the unknown. Methods Enzymol. 272, 315–326.

Grandel, H., Lun, K., Rauch, G.J., Rhinn, M., Piotrowski, T., Houart, C., Sordino, P., Kuchler, A.M., Schulte-Merker, S., Geisler, R., Holder, N., Wilson, S.W., Brand, M., 2002. Retinoic acid signalling in the zebrafish embryo is necessary during pre-segmentation stages to pattern the anterior–posterior axis of the CNS and to induce a pectoral fin bud. Development 129, 2851–2865.

Heine, U.I., Roberts, A.B., Munoz, E.F., Roche, N.S., Sporn, M.B., 1985. Effects of retinoid deficiency on the development of the heart and vascular system of the quail embryo. Virchows Arch., B Cell Pathol. Incl. Mol. Pathol. 50, 135–152.

Helms, J.A., Kim, C.H., Eichele, G., Thaller, C., 1996. Retinoic acid signaling is required during early chick limb development. Development 122, 1385–1394.

Higashijima, S., Hotta, Y., Okamoto, H., 2000. Visualization of cranial motor neurons in live transgenic zebrafish expressing green fluorescent protein under the control of the *Islet-1* promoter/enhancer. J. Neurosci. 20, 206–218.

Hill, J., Clarke, J.D., Vargesson, N., Jowett, T., Holder, N., 1995. Exogenous retinoic acid causes specific alterations in the development of the midbrain and hindbrain of the zebrafish embryo including positional respecification of the Mauthner neuron. Mech. Dev. 50, 3–16.

Holder, N., Hill, J., 1991. Retinoic acid modifies development of the midbrain–hindbrain border and affects cranial ganglion formation in zebrafish embryos. Development 113, 1159–1170.

Horton, C., Maden, M., 1995. Endogenous distribution of retinoids during normal development and teratogenesis in the mouse embryo. Dev. Dyn. 202, 312–323.

Idres, N., Marill, J., Flexor, M.A., Chabot, G.G., 2002. Activation of retinoic acid receptor-dependent transcription by all-*trans*-retinoic acid metabolites and isomers. J. Biol. Chem. 277, 31491–31498.

Johnson, S.L., Zon, L.I., 1999. Genetic backgrounds and some standard stocks and strains used in zebrafish developmental biology and genetics. Methods Cell Biol. 60, 357–359.

Knapik, E.W., Goodman, A., Ekker, M., Chevrette, M., Delgado, J., Neuhauss, S., Shimoda, N., Driever, W., Fishman, M.C., Jacob, H.J., 1998. A microsatellite genetic linkage map for zebrafish *Danio rerio*. Nat. Genet. 18, 338–343.

Kudoh, T., Wilson, S.W., Dawid, I.B., 2002. Distinct roles for Fgf, Wnt and retinoic acid in posteriorizing the neural ectoderm. Development 129, 4335–4346.

Linville, A., Ergi Gumusaneli, E., Chandraratna, R.A.S., Schilling, T.F., 2004. Independent roles for retinoic acid in segmentation and neuronal differentiation in the zebrafish hindbrain. Dev. Biol. 270, 186–199.

Masai, I., Lele, Z., Yamaguchi, M., Komori, A., Nakata, A., Nishiwaki, Y., Wada, H., Tanaka, H., Nojima, Y., Hammerschmidt, M., Wilson, S.W., Okamoto, H., 2003. N-cadherin mediates retinal lamination, maintenance of forebrain compartments and patterning of retinal neurites. Development 130, 2479–2494.

MacLean, G., Abu-Abed, S., Dolle, P., Tahayato, A., Chambon, P., Petkovich, M., 2001. Cloning of a novel retinoic-acid metabolizing cytochrome P450, Cyp26B1, and comparative expression analysis with Cyp26A1 during early murine development. Mech. Dev. 107, 195–201.

Nechiporuk, A., Finney, J.E., Keating, M.T., Johnson, S.L., 1999. Assessment of polymorphism in zebrafish mapping strains. Genome Res. 9, 1231–1238.

Nelson, D.R., 1999. A second CYP26 P450 in humans and zebrafish: CYP26B1. Arch. Biochem. Biophys. 371, 345–347.

Niederreither, K., Subbarayan, V., Dolle, P., Chambon, P., 1999. Embryonic retinoic acid synthesis is essential for early mouse post-implantation development. Nat. Genet. 21, 444–448.

Niederreither, K., Abu-Abed, S., Schuhbaur, B., Petkovich, M., Chambon, P., Dolle, P., 2002. Genetic evidence that oxidative derivatives of retinoic acid are not involved in retinoid signaling during mouse development. Nat. Genet. 31, 84–88.

Oosterveen, T., Niederreither, K., Dolle, P., Chambon, P., Meijlink, F., Deschamps, J., 2003. Retinoids regulate the anterior expression boundaries of 5′*Hoxb* genes in posterior hindbrain. EMBO J. 22, 262–269.

Perlmann, T., 2002. Retinoid metabolism: a balancing act. Nat. Genet. 31, 7–8.

Perz-Edwards, A., Hardison, N.L., Linney, E., 2001. Retinoic acid-mediated gene expression in transgenic reporter zebrafish. Dev. Biol. 229, 89–101.

Prince, V.E., Joly, L., Ekker, M., Ho, R.K., 1998a. Zebrafish *hox* genes: genomic organization and modified colinear expression patterns in the trunk. Development 125, 407–420.

Prince, V.E., Moens, C.B., Kimmel, C.B., Ho, R.K., 1998b. Zebrafish *hox* genes: expression in the hindbrain region of wild-type and mutants of the segmentation gene, *valentino*. Development 125, 393–406.

Sakai, Y., Meno, C., Fujii, H., Nishino, J., Shiratori, H., Saijoh, Y., Rossant, J., Hamada, H., 2001. The retinoic acid-inactivating enzyme CYP26 is essential for establishing an uneven distribution of retinoic acid along the anterior–posterior axis within the mouse embryo. Genes Dev. 15, 213–225.

Schilling, T.F., Piotrowski, T., Grandel, H., Brand, M., Heisenberg, C.P., Jiang, Y.J., Beuchle, D., Hammerschmidt, M., Kane, D.A., Mullins, M.C., van Eeden, F.J., Kelsh, R.N., Furutani-Seiki, M., Granato, M., Haffter, P., Odenthal, J., Warga, R.M., Trowe, T., Nusslein-Volhard, C., 1996. Jaw and branchial arch mutants in zebrafish I: branchial arches. Development 123, 329–344.

Schulte-Merker, S., van Eeden, F.J., Halpern, M.E., Kimmel, C.B., Nusslein-Volhard, C., 1994. *no tail* (*ntl*) is the zebrafish homologue of the mouse T (*Brachyury*) gene. Development 120, 1009–1015.

Sockanathan, S., Perlmann, T., Jessell, T.M., 2003. Retinoid receptor signaling in postmitotic motor neurons regulates rostrocaudal positional identity and axonal projection pattern. Neuron 40, 97–111.

Stratford, T., Horton, C., Maden, M., 1996. Retinoic acid is required for the initiation of outgrowth in the chick limb bud. Curr. Biol. 6, 1124–1133.

Swindell, E.C., Thaller, C., Sockanathan, S., Petkovich, M., Jessell, T.M., Eichele, G., 1999. Complementary domains of retinoic acid production and degradation in the early chick embryo. Dev. Biol. 216, 282–296.

Tahayato, A., Dolle, P., Petkovich, M., 2003. Cyp26C1 encodes a novel retinoic acid-metabolizing enzyme expressed in the hindbrain, inner ear, first branchial arch and tooth buds during murine development. Gene Expr. Patterns 3, 449–454.

Taimi, M., Helvig, C., Wisniewski, J., Ramshaw, H., White, J., Amad, M., Korczak, B., Petkovich, M., 2004. A novel human cytochrome P450, CYP26C1, involved in metabolism of 9-*cis* and all-*trans* isomers of retinoic acid. J. Biol. Chem. 279, 77–85.

Thisse, C., Thisse, B., Schilling, T.F., Postlethwait, J.H., 1993. Structure of the zebrafish *snail1* gene and its expression in wild-type, *spadetail* and *no tail* mutant embryos. Development 119, 1203–1215.

Tickle, C., Alberts, B., Wolpert, L., Lee, J., 1982. Local application of retinoic acid to the limb bond mimics the action of the polarizing region. Nature 296, 564–566.

Westerfield, M., 1995. *The Zebrafish Book*. University of Oregon Press, Salem, OR.

White, J.A., Guo, Y.D., Baetz, K., Beckett-Jones, B., Bonasoro, J., Hsu, K.E., Dilworth, F.J., Jones, G., Petkovich, M., 1996. Identification of the retinoic acid-inducible all-*trans*-retinoic acid 4-hydroxylase. J. Biol. Chem. 271, 29922–29927.

White, J.A., Ramshaw, H., Taimi, M., Stangle, W., Zhang, A., Everingham, S., Creighton, S., Tam, S.P., Jones, G., Petkovich, M., 2000a. Identification of the human cytochrome P450, P450RAI-2, which is predominantly expressed in the adult cerebellum and is responsible for all-*trans*-retinoic acid metabolism. Proc. Natl. Acad. Sci. U. S. A. 97, 6403–6408.

White, J.C., Highland, M., Kaiser, M., Clagett-Dame, M., 2000b. Vitamin A deficiency results in the dose-dependent acquisition of anterior character and shortening of the caudal hindbrain of the rat embryo. Dev. Biol. 220, 263–284.

Woods, I.G., Kelly, P.D., Chu, F., Ngo-Hazelett, P., Yan, Y.L., Huang, H., Postlethwait, J.H., Talbot, W.S., 2000. A comparative map of the zebrafish genome. Genome Res. 10, 1903–1914.

Yashiro, K., Zhao, X., Uehara, M., Yamashita, K., Nishijima, M., Nishino, J., Saijoh, Y., Sakai, Y., Hamada, H., 2004. Regulation of retinoic acid distribution is required for proximodistal patterning and outgrowth of the developing mouse limb. Dev. Cell 6, 411–422.